

# Dynamical effects of optical feedback in a laser diode with small $\alpha$ factor: an oasis of stability?

M. Sciamanna, P. Mégret and M. Blondel

Service d'Electromagnétisme et de Télécommunications, Faculté Polytechnique de Mons,  
31 Boulevard Dolez, B-7000 Mons, Belgium

*We find that a delayed feedback semiconductor laser may experience severe dynamical instabilities even when its  $\alpha$  factor is very small. New bifurcation mechanisms are unveiled when decreasing the  $\alpha$  factor, such as subcritical Hopf bifurcations leading to large intensity pulsating solutions, but also re-stabilization mechanisms of the first external-cavity mode.*

## Introduction

Optical feedback in semiconductor lasers, i.e. the retro-reflection of the emitted light into the laser cavity, has attracted a lot of attention owing to its practical importance as well as its rich and complex nonlinear dynamics [1]. Laser diodes with optical feedback are very often modelled by the single-mode Lang-Kobayashi (LK) equations [2, 3]:

$$\frac{dY}{ds} = (1 + i\alpha)ZY + \eta \exp(-i\Omega_0\theta)Y(s - \theta), \quad (1)$$

$$T\frac{dZ}{ds} = \bar{P} - Z - (1 + 2Z)|Y|^2, \quad (2)$$

where  $Y$  is the slowly varying amplitude of the electric field and  $Z$  is the carrier number in excess with respect to its threshold value.  $\alpha$  is the linewidth enhancement factor. The parameter  $T$  is defined as the ratio between the carrier lifetime  $\tau_s$  and the photon lifetime  $\tau_p$ , i.e.  $T \equiv \tau_s/\tau_p$ .  $\bar{P}$  is a normalized pump term.  $\theta \equiv \tau_{ext}/\tau_p$  is the external-cavity round-trip time  $\tau_{ext}$  normalized by  $\tau_p$ .  $\Omega_0 \equiv \omega_{th}\tau_p$ , where  $\omega_{th}$  is the frequency of the solitary laser at threshold.  $\eta \equiv f\tau_p$ , where  $f$  is the feedback rate. The steady states of the LK equations are the so-called external-cavity modes (ECMs) with  $Y = A_s \exp[i(\omega_s - \Omega_0)s]$  and  $Z = Z_s$ .  $A_s$ ,  $\omega_s$  and  $Z_s$  are three constant quantities.

The instabilities arising in delayed feedback laser diodes emerge from a cascade of bifurcations on the ECMs [4]. An ECM first destabilizes with a Hopf bifurcation and the emerging time-periodic solution eventually leads to more complex, possibly chaotic dynamics. Very often the Hopf bifurcations are supercritical, i.e. bifurcations to harmonic intensity solutions. However subcritical Hopf bifurcations leading to pulsating intensity solutions are also possible in the so-called short external-cavity (EC) regime [5], i.e. when the EC frequency is much larger than the RO frequency of the laser diode. Subcritical Hopf bifurcations are found in a large range of laser and feedback parameters but they usually disappear and become supercritical as  $\alpha$  decreases below  $\alpha \simeq 1$  [5].

The  $\alpha$  factor is an important parameter for semiconductor lasers. It is responsible for the enhancement of the laser linewidth and it influences the frequency chirp. In the search for high-frequency telecommunication systems, there is an increasing interest in small  $\alpha$  laser diodes [6] and in their optical feedback sensitivity. Previous studies have shown that a small  $\alpha$  laser diode would be more immune to feedback induced instabilities [5, 7, 8, 9]. In this paper, we show however that a small  $\alpha$  factor may also induce new bifurcation mechanisms and instabilities on the ECM steady-states, which are not present for conventional, large values of  $\alpha$ .

## Hopf bifurcation cascades and laser instabilities

As we increase  $\eta$ , ECMs are created in pairs and Hopf bifurcations progressively appear on the ECM steady states. We focus here on the first Hopf bifurcations that appear on the first ECM. We have characterized the Hopf bifurcations on the first ECM by the Hopf frequency  $\omega_H$  and the feedback rate  $\eta_H$  at which they occur. In Figs. 1 (a) and (b), we have plotted  $\eta_H$  and  $\omega_H/\omega_{RO}$  as a function of  $\theta$ , in the case of  $\alpha = 0.5$ .  $\eta_H$  and  $\omega_H$  have been computed numerically with the method explained in Ref. [5].  $\omega_{RO} \equiv \sqrt{2\bar{P}/T}$  is the RO frequency, here  $T_{RO} \equiv 2\pi/\omega_{RO} \simeq 170$ . The other parameters are fixed to  $\bar{P} = 1.155$ ,  $T = 1710$ ,  $\Omega_0\theta = \pi$  and  $\tau_p = 1$  ps. We distinguish different types of Hopf bifurcations. Stable Hopf bifurcation points are those that modify the stability of the

# Dynamical effects of optical feedback in a laser diode with small $\alpha$ factor: an oasis of stability?

ECM, either stabilizing or destabilizing it. They are supercritical (subcritical) if the emerging time-periodic solution is stable (unstable). Unstable attractors cannot be found with a direct integration of the rate equations. In order to discriminate between subcritical and supercritical Hopf points, we have therefore used another method based on the continuation package DDE-BIFTOOL [10], which allows to follow branches of steady-states and time-periodic solutions irrespective of their stability. Supercritical (subcritical) Hopf points are plotted in thick (dotted) line. By contrast, unstable Hopf bifurcations (dashed-dotted line) do not modify the ECM stability, i.e. they appear on always unstable ECMs.

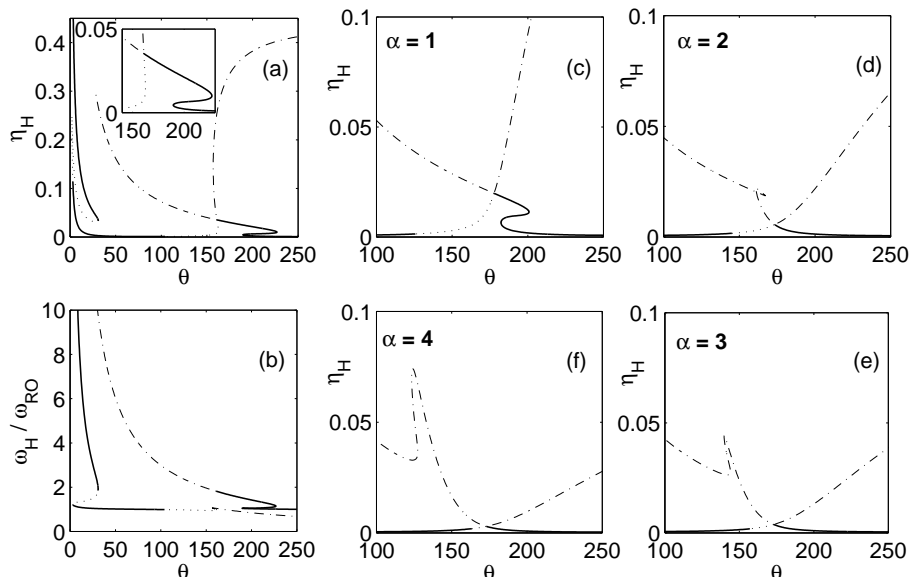


Figure 1: (a), (b): Analysis of the Hopf bifurcation curve in the planes  $(\theta, \eta_H)$  and  $(\theta, \omega_H/\omega_{RO})$  respectively, for  $\alpha = 0.5$ . The inset in (a) shows an enlargement of the Hopf curves. (c)-(f) same as (a) but for (c)  $\alpha = 1$ , (d)  $\alpha = 2$ , (e)  $\alpha = 3$ , (f)  $\alpha = 4$ .

As mentioned in our introduction, subcritical Hopf bifurcations are found in the short EC regime, that is, for a small  $\theta$  with respect to  $T_{RO}$ . Interestingly, another set of subcritical Hopf bifurcation points appears for  $110 \leq \theta \leq 165$ , i.e. close to the boundary with the long EC regime ( $\theta \simeq T_{RO}$ ). Moreover, the Hopf bifurcation curve exhibits two turning points. As a result, as we increase  $\eta$  the first ECM may experience two consecutive subcritical Hopf bifurcations (for  $\theta \simeq 160$ ) or two consecutive supercritical Hopf bifurcation points (for  $195 \leq \theta \leq 220$ ). The first Hopf bifurcation destabilizes the ECM and the second one re-stabilizes the ECM. In (c)-(f), we analyze the Hopf bifurcation curve as in (a) but for larger values of  $\alpha$ . If we compare (c)-(f) with (a), we can conclude that the increase of  $\alpha$  has dramatic consequences on the Hopf bifurcations. First, the sequence of two consecutive subcritical Hopf bifurcation points, which was observed close to  $\theta = 160$  in (a), is not present anymore when  $\alpha$  increases. Still we find subcritical Hopf bifurcation points but in a range of  $\theta$  that progressively decreases as we increase  $\alpha$ . Second, the sequence of three consecutive supercritical Hopf bifurcations, which was shown in (a) for  $\theta \simeq 195$ , disappears when  $\alpha$  increases above  $\alpha = 1$ . The subcritical Hopf points we analyze here and the cascade of subcritical or supercritical Hopf points associated with re-stabilization mechanisms are therefore strongly related to the small value of the  $\alpha$  factor.

Figure 2 analyzes the laser instability emerging from these Hopf bifurcations. In the left panel, we plot the intensity  $I \equiv |Y|^2$  of the first ECM steady states and their Hopf bifurcations ( $\diamond$ ) as a function of  $\eta$ . Apart from the first ECM, the other ECMs appear in pairs as  $\eta$  increases. In solid (dashed) line is shown the stable (unstable) part of each branch. Bold  $\diamond$  indicate the Hopf bifurcation points that modify the stability of the first ECM [they belong to the solid or dotted lines in Fig. 1 (a)]. In the right panel are shown some branches of time-periodic solutions emerging from the Hopf bifurcation points. The stable (unstable) parts of the branches of time-periodic solutions are shown in solid (dashed) lines. The time-periodic solutions may destabilize either from a torus bifurcation (\*), from a limit point ( $\square$ ), or from a period doubling bifurcation ( $\triangle$ ).

Figures 2 (a), (b) illustrate the ECM stability when  $\theta = 160$ . As we increase  $\eta$  from zero, the first ECM destabilizes from a subcritical Hopf bifurcation point and remains unstable if we further increase  $\eta$ . From the subcritical Hopf bifurcation point emerges an unstable branch of time-periodic solution, which grows in amplitude as we decrease  $\eta$  and coexists with the steady state branch of the first ECM. The stability of the branch of time-periodic solution is determined by a limit point for small  $\eta$  and by a torus bifurcation for larger  $\eta$ .

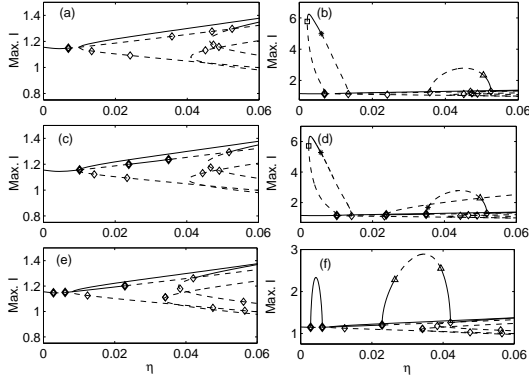


Figure 2: Bifurcation diagram of the intensity  $I$  for the first branches of ECMs as a function of the feedback rate  $\eta$ , for  $\theta = 160$  (a), (b),  $\theta = 162$  (c), (d),  $\theta = 195$  (e),(f).

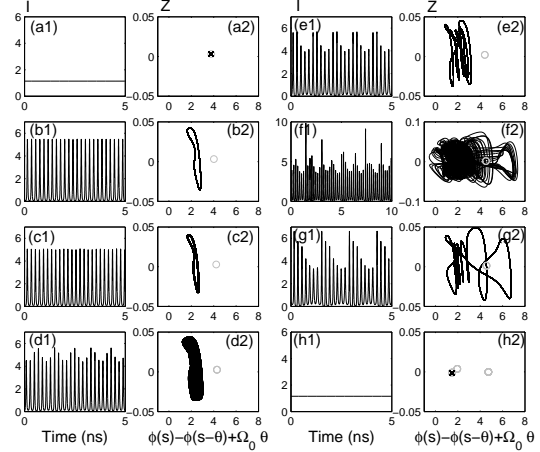


Figure 3: Time-traces of  $I$  and system trajectory in the phase plane  $[\phi(s) - \phi(s - \theta) + \Omega_0\theta, Z]$ , for (a1), (a2)  $\eta = 0.00400$ , (b1), (b2)  $\eta = 0.00500$ , (c1), (c2)  $\eta = 0.00602$ , (d1), (d2)  $\eta = 0.00640$ , (e1), (e2)  $\eta = 0.00720$ , (f1), (f2)  $\eta = 0.00790$ , (g1), (g2)  $\eta = 0.00830$ , (h1), (h2)  $\eta = 0.01000$ . The other parameters are as in Figs. 2 (a), (b).

Figure 3 analyzes in more details the laser dynamics emerging from the subcritical Hopf bifurcation point. We plot the time-trace of  $I$  together with the system trajectory in the plane  $[\phi(s) - \phi(s - \theta) + \Omega_0\theta, Z]$ , for several increasing values of  $\eta$ .  $\phi(s)$  is the phase of the field  $Y(s) \equiv |Y| \exp[i\phi(s) - i\Omega_0s]$ . The circles represent the ECM steady states. In (a1), (a2), the laser exhibits a steady state corresponding to the first ECM. As we increase  $\eta$ , the first ECM undergoes a subcritical Hopf bifurcation and the laser then jumps to a large limit cycle attractor (b2), which corresponds to the emission of sharp, large intensity pulses with a frequency close to the RO frequency (b1). Indeed, as shown in Fig. 1 (b), the Hopf frequency  $\omega_H$  of the subcritical Hopf bifurcation is close to  $\omega_{RO}$ . As shown in Fig. 2 (b), the time-periodic solution emerging from the subcritical Hopf bifurcation destabilizes for larger values of  $\eta$  with a torus bifurcation. In (c1), (c2) the phase space trajectory exhibits a "noisy" attractor that results from the combination of the fast pulsating behavior with a slower envelope modulation. For still larger  $\eta$ , the modulation depth increases and the laser system exhibits a typical quasiperiodic oscillation with a slow modulation of fast intensity pulses [(d1), (d2)]. As we increase  $\eta$  the window of quasiperiodic oscillations is interspersed with windows of time-periodic oscillations [(e1), (e2)]. For  $\eta = 0.00790$  (f1), (f2), the time-periodic solution may bifurcate to a chaotic-like dynamics, in which the intensity exhibits irregular bursts of fast intensity pulses (f1). For larger  $\eta$ , the windows of chaotic-like intensity oscillations are interspersed with windows of time-periodic oscillations [(g1), (g2)]. As we increase  $\eta$  further, a new pair of ECMs is created and the system locks to the mode with the maximum gain (the smaller  $Z$ ) [(h1), (h2)].

The Hopf bifurcation points appearing for larger values of  $\eta$  on the first branch of ECM in Figs. 2 (a),(b) are unstable. The branches of time-periodic solutions emerging from these Hopf points are therefore also unstable but they may stabilize as we increase the bifurcation parameter [see Fig. 2 (b) close to  $\eta = 0.035$ ]: a branch of time-periodic solution connects an unstable Hopf point on the first ECM to a supercritical Hopf point on the high-intensity branch of the next ECM.

The re-stabilization mechanisms of the first ECM [unveiled in Fig. 1 (a) close to the turning points in the Hopf curve] are illustrated in Figs. 2 (c), (d) and Figs. 2 (e), (f).

# Dynamical effects of optical feedback in a laser diode with small $\alpha$ factor: an oasis of stability?

Figures 2 (c) and (d) analyze the case  $\theta = 162$ , for which the first ECM re-stabilizes with a subcritical Hopf bifurcation. As we increase  $\eta$ , the first ECM destabilizes from a subcritical Hopf bifurcation and by contrast to (a), (b), the first ECM re-stabilizes from a second subcritical Hopf bifurcation for a larger  $\eta$ . A third, supercritical Hopf bifurcation point, appears for larger values of  $\eta$  and definitely destabilizes the first ECM steady state. The branch of time-periodic solution emerging from the first subcritical Hopf bifurcation point is very similar to that of (b). The branch of time-periodic solution emerging from the second subcritical Hopf bifurcation point connects to a saddle-type ECM (antimode) at much larger values of  $\eta$  [out of the range of  $\eta$  in Fig. 2 (d)] and it never stabilizes. Finally, the branch of time-periodic solution emerging from the third, supercritical Hopf bifurcation on the first ECM destabilizes as we increase  $\eta$  through a torus bifurcation and re-stabilizes for larger values of  $\eta$  through an inverse period doubling bifurcation ( $\Delta$ ). It then connects a supercritical Hopf bifurcation on the mode branch of a next ECM.

Figures 2 (e), (f) illustrate the case  $\theta = 195$ , for which the first ECM re-stabilizes with a supercritical Hopf bifurcation. As we increase  $\eta$ , the first ECM destabilizes from a supercritical Hopf bifurcation, then re-stabilizes from a second supercritical Hopf bifurcation and for larger values of  $\eta$  the first ECM destabilizes from a third supercritical Hopf bifurcation. The branches of time-periodic solutions plotted in Fig. 2 (f) show that, interestingly, a completely stable branch of time-periodic solution connects the first ECM to itself for small values of  $\eta$ . To the best of our knowledge, such a cascade of supercritical Hopf bifurcations on the first ECM is shown here for the first time. The frequency of the laser intensity modulation is close to the RO frequency, in agreement with the Hopf frequency we computed in Fig. 1 (b). Another branch of time-periodic dynamics is shown in Fig. 2 (f) for larger  $\eta$ . This branch emerges from the third Hopf bifurcation and its stability is determined by two period-doubling bifurcations. By contrast to the time-periodic oscillations that appear for a smaller value of  $\eta$ , the frequency of the intensity oscillations is not related to the RO frequency and is about twice the RO frequency. Indeed, as shown in Fig. 1 (b), the Hopf frequency  $\omega_H$  of the third supercritical Hopf bifurcation is much larger than  $\omega_{RO}$ . As we have shown elsewhere [5], the time-periodic solution associated to such a bridge of supercritical Hopf bifurcations for large values of  $\eta$  corresponds physically to a beating between two ECMs. Interestingly, this oscillatory behavior with a high frequency is obtained in an all optical way, i.e. without the need of any expensive fast electronics.

## Conclusions

In summary, we have shown that a small  $\alpha$  factor may be responsible for new Hopf bifurcation instabilities in delayed laser diodes. The laser may exhibit subcritical Hopf bifurcations which are associated with strongly pulsating, large intensity, laser outputs. Moreover, we have unveiled re-stabilization mechanisms of the first ECM through subcritical or supercritical Hopf bifurcations. The cascade of Hopf bifurcations related to these re-stabilization mechanisms disappears when the  $\alpha$  factor increases.

*M. S. is a Research Fellow from FNRS (Belgium). The authors acknowledge the support from the IAP program of the Belgian Government.*

## References

- [1] K. Petermann, IEEE J. Sel. Top. Quantum Electron. **1**, 480 (1995).
- [2] R. Lang and K. Kobayashi, IEEE J. Quantum Electron. **16**, 347 (1980).
- [3] P. Alsing, V. Kovanis, A. Gavrielides, and T. Erneux, Phys. Rev. A **53**, 4429 (1996).
- [4] A. Hohl and A. Gavrielides, Phys. Rev. Lett. **82**, 1148 (1999).
- [5] M. Sciamanna, T. Erneux, A. Gavrielides, V. Kovanis, P. Mégret, and M. Blondel, in *Physics and Simulation of Optoelectronics Devices XI*, eds. M. Osinski, H. Amano, P. Blood, SPIE Proc. **4986**, pp. 469-479 (2003).
- [6] T.C. Newell, D.J. Bossert, A. Stintz, B. Fuchs, K.J. Malloy, and L.F. Lester, IEEE Photonics Technol. Lett. **11**, 1527 (1999).
- [7] B. Tromborg and J. Mork, IEEE J. Quantum Electron. **26**, 642 (1990).
- [8] T. Heil, I. Fischer, and W. Elsasser, Phys. Rev. A **60**, 634 (1999).
- [9] T. Erneux, A. Gavrielides, and M. Sciamanna, Phys. Rev. A **66**, 033809 (2002).
- [10] K. Engelborghs, T. Luzyanina, and D. Roose, Tech. Rep. TW-330, Department of Computer Science, Katholieke Universiteit Leuven, Belgium (Software available at <http://www.cs-kuleuven.ac.be/~koen/delay/ddebiftool.shtml>) (2000).